Circularly polarized lasing in chiral modulated semiconductor microcavity with GaAs quantum wells

A. A. Demenev,[1] V. D. Kulakovskii,[1] C. Schneider,[2] S. Brodbeck,[2] M. Kamp,[2] S. Höfling,[2,3] S. V. Lobanov,[4] T. Weiss,[5] N. A. Gippius,[6,7] and S. G. Tikhodeev[7,1,8,a)]

[1)] *Institute of Solid State Physics, Russian Academy of Science, Chernogolovka 142432, Russia*

[2)] *Technische Physik and Wilhelm-Conrad-Röntgen-Research Center for Complex Material Systems, Universität Würzburg, D-97074 Würzburg, Am Hubland, Germany*

[3)] *SUPA, School of Physics and Astronomy, University of St Andrews, St Andrews, KY16 9SS, United Kingdom*

[4)] *School of Physics and Astronomy, Cardiff University, Cardiff CF24 3AA, United Kingdom*

[5)] *4th Physics Institute and Research Center SCoPE, University of Stuttgart, Stuttgart D-70550, Germany*

[6)] *Skolkovo Institute of Science and Technology, Novaya Street 100, Skolkovo 143025, Russia*

[7)] *A. M. Prokhorov General Physics Institute, Russian Academy of Sciences, Vavilova Street 38, Moscow 119991, Russia*

[8)] *M. V. Lomonosov Moscow State University, Leninskie Gory 1, Moscow 119991, Russia*

(Dated: 11 October 2016)

We report the elliptically, close to circularly polarized lasing at $\hbar\omega = 1.473$ and 1.522 eV from an AlAs/AlGaAs Bragg microcavity with 12 GaAs quantum wells in the active region and chiral-etched upper distributed Bragg refractor under optical pump at room temperature. The advantage of using the chiral photonic crystal with a large contrast of dielectric permittivities is its giant optical activity, allowing to fabricate a very thin half-wave plate, with a thickness of the order of the emitted light wavelength, and to realize the monolithic control of circular polarization.

PACS numbers: 71.36.+c, 42.65.Pc, 42.55.Sa

Modern nanofabrication technologies allow to realize photonic structures — photonic crystals and metamaterials — with extraordinary optical properties[1–3]. In particular, chiral photonic structures are known to demonstrate a giant optical activity, several orders of magnitude stronger than natural materials[4–9]. Recently, it has been demonstrated that incorporating a chiral photonic structure into a planar GaAs waveguide or a semiconductor microcavity (MC) with embedded light-emitting achiral InAs quantum dots (QD) allows to achieve light emission with a high degree of circular polarization (DCP), without applying magnetic field and without the need of thick quarter-waveplates[10–12]. The effect is due to the modification of the symmetry and density of environmentally allowed electromagnetic modes relative to that in free space due to the chiral nanostructuring, which, in turn, affects the spontaneous emission rate, directional pattern, and polarization[13,14]. This method has considerable advantages: small size, very simple operation, and compatibility with semiconductor fabrication process. In this Letter we demonstrate that the method works for the stimulated emission as well, and demonstrate a highly circularly polarized lasing from an AlGaAs/AlAs microcavity with chirally etched top Bragg mirror with GaAs quantum wells (QW) in the active cavity. Previously, the elliptically polarized lasing with a good DCP was realized on a quantum cascade laser with monolithic control of circular polarization in the THz range of frequencies[15].

A chiral photonic crystal (CPC), a monolithic part of the upper cavity mirror, is fabricated from the AlAs/AlGaAs/GaAs high Q-factor MC grown by molecular beam epitaxy on a (001)-oriented GaAs. The full planar cavity consists of a lower and an upper Bragg reflectors with 27 and 23 pairs of AlAs/$Al_{0.20}Ga_{0.80}As$ layers, respectively, with 3 nm GaAs smoothing layer after each pair in the Bragg reflectors and an active layer with three groups of four 13 nm GaAs QWs separated by 4 nm AlAs bariers. The nominal thicknesses of the AlAs and $Al_{0.20}Ga_{0.80}As$ layers in Bragg mirrors are (68 ± 3) nm and (58 ± 3) nm, respectively. The Bragg pairs are deposited on the wafer with a slight wedge from the center to the circumference, resulting in a blueshift of the cavity resonance which can amount up to ≈200 meV. It consists of the central group of four GaAs QWs with three AlAs barriers between them, surrounded by 32 nm AlAs and 26 nm $Al_{0.20}Ga_{0.80}As$ layers, and symmetric siding groups of four AlAs/GaAs barier/QW layers with 28 nm AlAs trailing layers, see in Supplementary Material.

A chiral layer is fabricated by electron-beam nanolithography and dry etching through top $N_{\text{etch}} = 4.75$ Bragg pairs of the upper mirror (which means through the four top Bragg pairs, the AlAs layer and 1/2 of the $Al_{0.20}Ga_{0.80}As$ layer of the 5th Bragg pair). The

a)tikh@gpi.ru

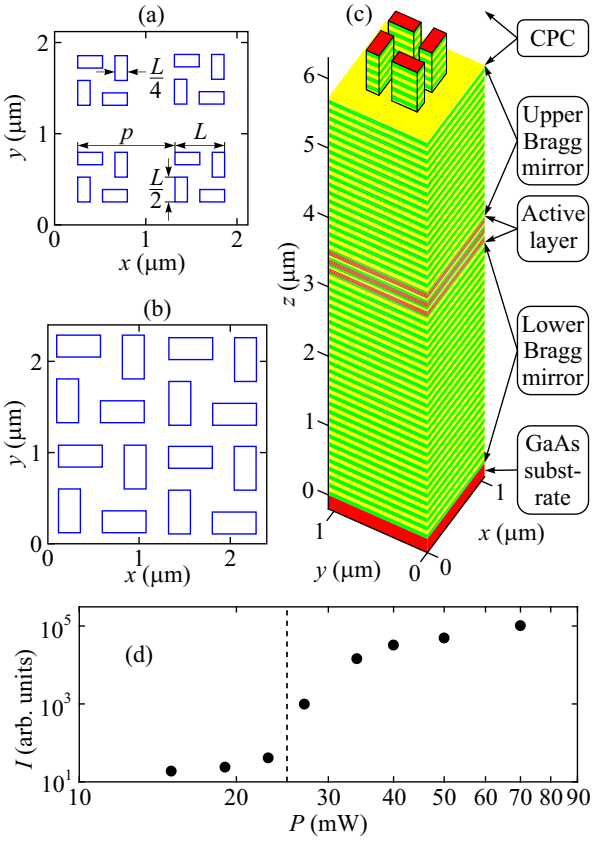

FIG. 1. (color online). (a,b) The schematics of chiral photonic crystal (CPC) composed of a square lattice of rectangular nanopillars in Sample A (panel a) and B (panel b), 2×2 periods are shown. (c) The schematics of the unit cell of Sample A. The nanopillars, composing the CPC, are etched through the top 4.75 (of 23) Bragg pairs of the upper Bragg mirror of a planar AlGaAs/AlAs microcavity with twelve GaAs QWs (three groups of four). Green and yellow colors represent AlAs and AlGaAs $\lambda/4$-layers, respectively. Red color represents GaAs substrate, smoothing layers between Bragg pairs and active QWs. (d) Measured emission intensity of Sample A I as a function of the optical pump intensity P.

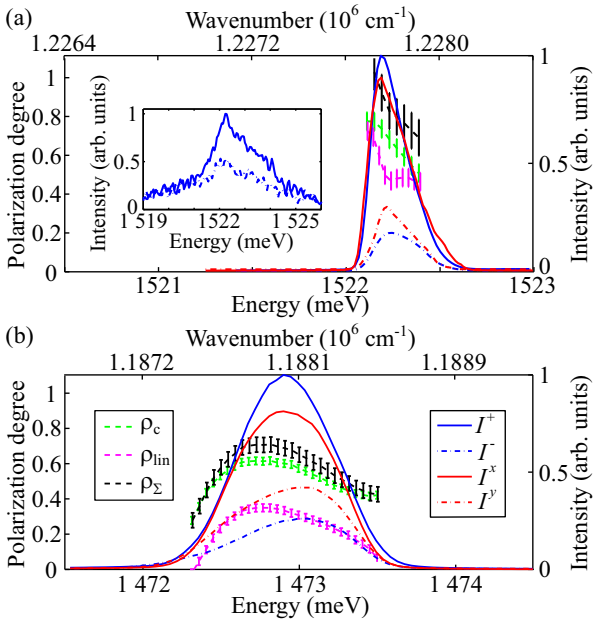

FIG. 2. (color online). (a) The emission intensity spectra of Sample A at $T = 300$ K at pump intensity above the threshold, at $P \approx 2P_{\rm thr}$, in circular $I^{\pm}$ (blue solid and dash-dotted lines) and linear $I^{x,y}$ (red lines) polarizations. Green, magenta, and black lines with errorbars show the circular, linear, and total polarization degrees, $\rho_{\rm c}$, $\rho_{\rm lin}$, ρ_Σ, respectively. (b) Same for Sample B. The insert in panel (a) shows the emission spectra in circular polarizations $I^{\pm}$ in Sample A slightly below the threshold, at $P = 0.95P_{\rm thr}$.

schematics of the CPC is depicted in Fig. 1, see also in Supplementary Material. It consists of a square lattice of rectangular pillars that have a broken in-plane mirror symmetry but possess a fourfold rotational axis and possess the potential to demonstrate a strong optical activity[16]. The vertical walls of nanopillars are normal to the [110] and [$\bar{1}$10] crystallographic directions. This structure has a C_4 point symmetry, and it is three-dimensionally chiral, because it does not have planes of mirror symmetry, including the horizontal one[6].

Two different periodic structures (Sample A and B hereafter) have been fabricated, basing on the theoretical calculations explained below and shown schematically in Figs. 1a and 1b. Sample A (panel a) has the period $p = 1060$ nm and pillar feature size $L = 544$ nm, and Sample B (panel b) has $p = 1200$ nm and $L = 960$ nm. The horizontal size of chiral structure in each sample is approximately $50 \times 50\,\mu$m^2. The Samples A and B are cleaved from different horizontal parts of the wafer, and show different photon energies of the main MC mode, around 1523 and 1473 meV at room temperature, respectively.

The samples are held at room temperature. The excitation is carried out with a Ti-sapphire laser in the spectral range of the first reflection minimum of the MC. The laser spot has a diameter of about 10 μm. The emission is collected in an angle range of $\pm 15°$. It is dispersed by a monochromator and detected by a Si CCD camera. The polarization of the luminescence is analyzed by a quarter wave retarder and linear polarizers.

The emission intensity from both samples at low pump intensities depends weakly on the angle, its spectral width reaches a few meV. With increase in the excitation power the emission spectrum and intensity show a threshold-like transition to lasing regime at $P = P_{\rm thr}$, see Fig. 1d for Sample A. Above the threshold the emission line becomes narrow. The full width at half maximum is about 0.23 meV at $P = 1.1P_{\rm thr}$ and increases to ~ 0.5 meV at $P = 2.5P_{\rm thr}$. Figures 2a and b display the measured emission intensities (from Samples A and B, respectively) in two circular (I^+, I^-) and two linear (I^x, I^y) polarizations as functions of photon energy $\hbar\omega$, at the normal to the MC plane at $P \sim 2P_{\rm thr}$ and zero

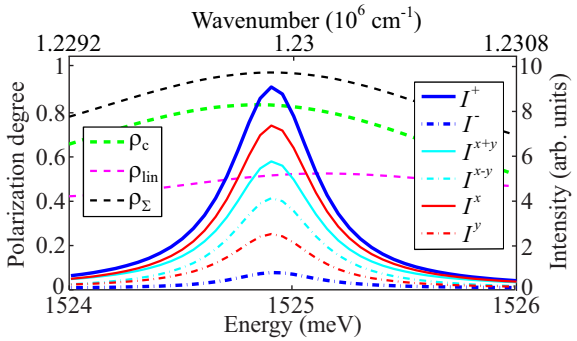

FIG. 3. (color online). Calculated (for Sample A) emission intensity spectra in right- and left-circular polarizations (thick blue solid and dash-dotted lines). The corresponding circular polarization degree spectra is shown by thick dashed green line. Red and cyan lines show the linearly polarized (in xy and diagonal directions respectively) intensities $I^x, I^y, I^{x+y}, I^{x-y}$, calculated assuming that all oscillating dipoles are aligned along diagonal $x+y$ direction. The resulting linear and total polarization degrees $\rho_{\rm lin}$ and ρ_Σ are shown as magenta and black dashed lines. It can be seen that the linear polarization is predominantly along x direction.

magnetic field. (The emission intensities in two diagonal linear polarizations $x \pm y$ are not shown as they differ very weakly from each other.) The dashed lines in Figs. 2a and b show the degrees of circular, linear, and total polarization defined as

$$\rho_c = \frac{I^+ - I^-}{I^+ + I^-}, \rho_{xy} = \frac{I^x - I^y}{I^x + I^y}, \rho_{x\pm y} = \frac{I^{x+y} - I^{x-y}}{I^{x+y} + I^{x-y}},$$
$$\rho_{\rm lin} = \sqrt{\rho_{xy}^2 + \rho_{x\pm y}^2}, \rho_\Sigma = \sqrt{\rho_c^2 + \rho_{\rm lin}^2}. \quad (1)$$

It is seen that in Sample A the lasing is nearly completely elliptically polarized, with polarization degrees at the intensity maxima as large as $\rho_c \sim 80\%$, $\rho_{\rm lin} \sim 50\%$, and $\rho_\Sigma \sim 95\%$ (Fig. 2a). The polarization of emission in Sample B (Fig. 2b) is smaller, $\rho_c \sim 60\%$, $\rho_{\rm lin} \sim 35\%$, and $\rho_\Sigma \sim 80\%$. This is in agreement with a significantly broader linewidth of the emission from Sample B, compare Figs. 2a and b.

The reciprocity and symmetry analysis of the structure shows that the CPC in the structures works as a waveplate, exploring the Fabry-Perot interference between the vertically propagating modes in the slab, which allows reaching nearly a 100% circular polarization of the transmission[11]. To optimize the chiral structures for obtaining a high DCP of light emission we have calculated the frequency dependence of emission in right and left circular polarizations, using the optical scattering matrix and Fourier modal method[10–12,17]. In this approximation the emission is calculated actually for homogeneously distributed oscillating point dipoles in the QW plane, which are driven by external excitation and emit incoherently, so that the intensities rather than the electromagnetic fields are summed up at the receiver. This approximation (so called weak coupling limit) is not completely valid for describing the lasing. But below and slightly above the threshold of the lasing regime it might be a reasonable starting point for optimization of the structures.

In this approximation, assuming the overall C_4 symmetry of the system, only a circular polarization of emission can be expected. The linear polarization is absent, because the oscillating dipoles are assumed to be randomly linearly polarized in xy plane. The calculated emission intensities in right and left circular polarizations $I^\pm$ for a structure with parameters of Sample A are shown in Fig. 3 as blue solid and dash-dotted lines. The intensities are normalized to the emission intensity of the same oscillating dipoles in vacuum. The resulting dependence of $\rho_c(\hbar\omega)$ is shown in Fig. 3 by the dashed green line. It can be seen that the emission is expected to be strongly circularly polarized, with ρ_c up to 80%, in agreement with the experiment. For details on the simulated linearly polarized components, see our explanations below, after discussion of the important features of the circular polarization control by CPC .

Additional insight into the mechanism of circularly polarized emission is provided in Fig. 4 with the calculated spatial distribution of the circularly polarized emission intensity in Sample A at the resonant frequency $\hbar\omega = 1.522$ eV, as well as the spatial distribution of the DCP of emission $\rho_c(x,y)$, over the CPC unit cell. We would like to emphasize that Fig. 5 does not show the emission intensity distributions in a certain plane above the sample, but the spatial distributions of the emission effectiveness from different spatial points of the sample unit cell in the normal direction of the structure. These spatial distributions are connected via the electrodynamic reciprocity principle with the local electric field distributions in the active material plane inside the structure, produced by a normally incident planar wave of the corresponding polarization[11].

Note that ρ_c is very sensitive to the etching depth[12]. Figure 5 shows the calculated dependence of the maximum ρ_c of emission from Samples A (solid line) and B (dash-dotted line) as functions of etching depth $N_{\rm etch}$ (measured in the number of etched Bragg pairs). Thus, the structures employed in our experiments with $N_{\rm etch} \sim 4.75$ are in agreement with these calculations, corresponding to the maxima of the expected ρ_c.

Figure 2 shows that the measured emission in the lasing mode shows as well a pronounced linear polarization along x direction in Fig. 1c, i.e., along the (110) crystallographic direction of the AlGaAs and GaAs layers. There are two possible explanations: 1. The lasing operation itself, with possible preferential stimulated alignment of oscillating dipoles along a defined polarization direction. 2. The operation of the CPC, where possible fabrication-induced deformation of the CPC structures could lead to a reduced structural symmetry.

Although the lasing operation is not included in the simulation model, it is possible to check the effect of possible preferential alignment of oscillating dipoles. Red and cyan lines in Fig. 3 show the calculated emission

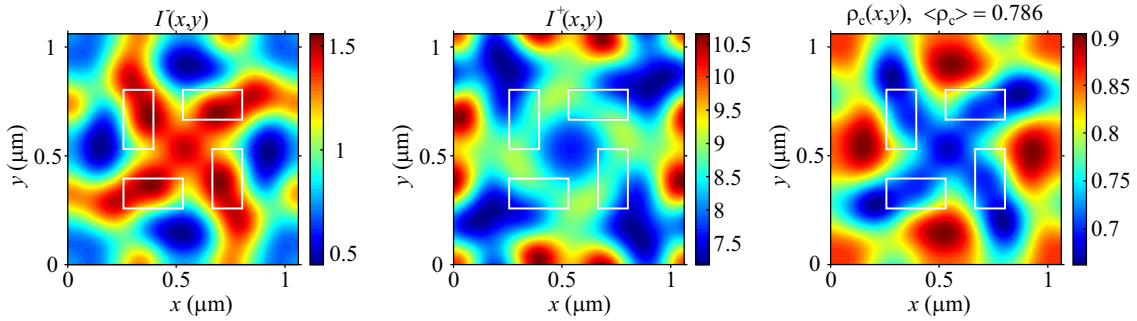

FIG. 4. (color online). Calculated spatial emission intensity distributions in Sample A in left ($I^-(x,y)$) and right ($I^+(x,y)$) circular polarizations (left and central panels), and spatial distribution of circular polarization degree $\rho_c(x,y)$ (right panel).

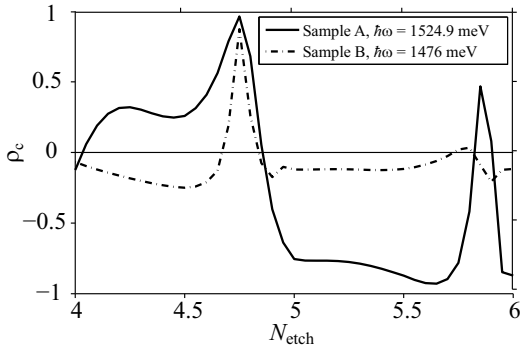

FIG. 5. Calculated dependencies of maximum circular polarization degree ρ_c on etching depth $N_{\rm etch}$ (measured as the number of etched Bragg pairs) for Sample A (solid line) and Sample B (dash-dotted line) structures.

intensities $I^{x,y}, I^{x\pm y}$ in linear xy and diagonal polarizations, assuming that all oscillating dipoles are aligned along diagonal $x+y$ direction. The linear polarization degree $\rho_{\rm lin}$ and total polarization degree ρ_Σ are shown as magenta and black dashed lines in Fig. 3. It is seen that the alignment of the oscillating dipoles leads to a pronounced linear x polarization, as in the experiment.

As to the possible fabrication-induced deformation of the CPC structures, they may cause the linear polarization of emission as well, see in Supplementary Material. However, the DCP in this case is usually less than in the perfect structure.

To conclude, we have found that fabricating chiral photonic crystals with light emitting GaAs quantum wells inside a planar MC allows to realize lasing with a high degree of circular polarization of the light emission in the absence of a magnetic field. The advantage of using the CPCs with a large contrast of dielectric permittivities is its giant optical activity. This allows one to fabricate a very thin "waveplate", with a thickness of the order of the emitted light wavelength. One more advantage of CPC half-wave plates lies in the fact that they, unlike the traditional ones, have in-plane rotational isotropy due to the C_4 symmetry. Thus, our chiral structures do not require linearly polarized emission of the active material at some precise polarization direction, which is an important advantage of the demonstrated approach over conventional quarter-wave plates.

Supplementary Material at [URL will be inserted by AIP] contains a more detailed description of the cavity design and the influence of possible fabrication-induced deformation of the CPC structures on the linear polarization of emission.

Acknowledgement. This work has been funded by Russian Scientific Foundation (grant 14-12-01372) and State of Bavaria. We are grateful to K. Konishi, L. Kuipers, M. Kuwata-Gonokami, R. Oulton, H. Tamaru, and F. Capasso for fruitful discussions, and M. Emmerling for preparing the nanopillars.

[1] E. Yablonovitch, Phys. Rev. Lett. **58**, 2059 (1987).
[2] S. Fan, P. R. Villeneuve, J. Joannopoulos, and E. F. Schubert, Phys. Rev. Lett. **78**, 3294 (1997).
[3] E. Miyai, K. Sakai, T. Okano, W. Kunishi, D. Ohnishi, and S. Noda, Nature **441**, 946 (2006).
[4] A. Papakostas, A. Potts, D. M. Bagnall, S. L. Prosvirnin, H. J. Coles, and N. I. Zheludev, Phys. Rev. Lett. **90**, 107404 (2003).
[5] M. Kuwata-Gonokami, N. Saito, Y. Ino, M. Kauranen, K. Jefimovs, T. Vallius, J. Turunen, and Y. Svirko, Phys. Rev. Lett. **95**, 227401 (2005).
[6] D.-H. Kwon, P. L. Werner, and D. H. Werner, Opt. Express **16**, 11802 (2008).
[7] N. Liu, H. Liu, S. Zhu, and H. Giessen, Nat. Photon. **3**, 157 (2009).
[8] M. Hentschel, L. Wu, M. Schäferling, P. Bai, E. P. Li, and H. Giessen, ACS Nano **6**, 10355 (2012).
[9] X. Yin, M. Schäferling, B. Metzger, and H. Giessen, Nano Letters **13**, 6238 (2013)..
[10] A. A. Maksimov, I. I. Tartakovskii, E. V. Filatov, S. V. Lobanov, N. A. Gippius, S. G. Tikhodeev, C. Schneider, M. Kamp, S. Maier, S. Höfling, and V. D. Kulakovskii, Phys. Rev. B **89**, 045316 (2014).
[11] S. V. Lobanov, T. Weiss, N. A. Gippius, S. G. Tikhodeev, V. D. Kulakovskii, K. Konishi, and M. Kuwata-Gonokami, Opt. Lett. **40**, 1528 (2015).
[12] S. V. Lobanov, S. G. Tikhodeev, N. A. Gippius, A. A. Maksimov, E. V. Filatov, I. I. Tartakovskii, V. D. Kulakovskii, T. Weiss, C. Schneider, J. Geßler, M. Kamp, and S. Höfling, Phys. Rev. B **92**, 205309 (2015).
[13] K. Konishi, M. Nomura, N. Kumagai, S. Iwamoto, Y. Arakawa, and M. Kuwata-Gonokami, Phys. Rev. Lett. **106**, 057402 (2011).
[14] N. Shitrit, I. Yulevich, E. Maguid, D. Ozeri, D. Veksler, V. Kleiner, and E. Hasman, Science **340**, 724 (2013).

[15] P. Rauter, J. Lin, P. Genevet, S. P. Khanna, M. Lachab, A. Giles Davies, E. H. Linfield, and F. Capasso, Proceedings of the National Academy of Sciences **111**, E5623 (2014).
[16] K. Konishi, B. Bai, X. Meng, P. Karvinen, J. Turunen, Y. P. Svirko, and M. Kuwata-Gonokami, Opt. Express **16**, 7189 (2008).
[17] D. M. Whittaker and I. S. Culshaw, Phys. Rev. B **60**, 2610 (1999).